ChemComm

COMMUNICATION

View Article Online
View Journal | View Issue

Cite this: *Chem. Commun.*, 2025, **61**, 16822

Received 17th July 2025,
Accepted 24th September 2025

DOI: 10.1039/d5cc04045k

rsc.li/chemcomm

Operando fluorescence lifetime imaging microscopy during Li^+ intercalation into graphitic electrodes

Matthew J. Quarrell, [a] Thukshan Samarakoon, [a] Alex R. Neale, [a] Oliver J. Barker, [a] Stanley W. Botchway [b] and Laurence J. Hardwick *[ac]

The evolution of emission background within Li-ion half-cells was monitored using *operando* fluorescence lifetime imaging microscopy. Fluorescence lifetimes were spatially mapped on graphite electrodes during lithiation and delithiation within two electrolyte formulations containing either a $Li[PF_6]$ or $Li[ClO_4]$ salt, which highlighted differing emission characteristics associated with salt stability.

The demand for Li-ion cells is predicted to reach 2600 GWh by 2030, which has initiated significant effort to develop longer-life cells.[1] Therefore, understanding key chemical processes occurring within the cell during operation in real time is of significant importance and a wide variety of *ex situ* and *operando* methods have been utilised to study these in great detail.[2–4] Raman spectroscopy is one such method being used extensively to monitor the surface region and interfaces upon electrode materials and local structural changes under potential control.[5–10] Over the years, studies have commented on the changing emission background during *ex situ* and *operando* Raman measurements, highlighting the varying fluorescent properties of species within the electrolyte and those present at the electrode surface.[11–16] To understand the origin of the emission background in Li-ion cells, a preliminary *in situ* investigation utilising fluorescence lifetime imaging microscopy (FLIM) comparing an uncycled and cycled graphite electrode showed a range of fluorescence lifetime processes.[11]

Fluorescence lifetime is the measure of time an electron is in an excited state by monitoring the time taken for the fluorescence to decay to 36% of the original value.[17] FLIM generates lifetime values on a pixel-by-pixel basis to create 2D and 3D images of the fluorescing species and has seen extensive use in the biological sciences where samples are either endogenous or able to be tagged with fluorescent species from uranium oxidation to important biomolecules, but has yet to be applied to electrochemical systems.[18–20] FLIM has the advantage that the measurement, unlike steady-state optical fluorescence microscopy, allows for the monitoring of changing environments by exploiting differences in excited state fluorescence lifetime as a function of the species environment, and therefore, the addition of a dye is not always necessary where autofluorescence is present. FLIM is capable of distinguishing between differing fluorophores independent of the intensity (and wavelength) of fluorescence of the fluorophores, allowing for the detection of multiple species simultaneously.[17,18] By being able to detect multiple species at once, FLIM provides the opportunity to monitor fluorescence changes that occur at potentials associated with the formation of the solid electrolyte interphase (SEI). The SEI comprises a heterogenous mixture of reaction products (*e.g.*, inorganic salts: LiF, Li_2O, and Li_2CO_3 and organic compounds: polymers/polycarbonates which form on graphite electrodes in Li-ion cells). The SEI acts as an important barrier to further electrolyte reduction, whilst allowing Li^+ transport.[21,22]

Fluorescence can be used to monitor cross talk between electrodes, an example of this is the use of *operando* steady-state optical fluorescence microscopy for the study of lithium sulfur (Li–S) cell chemistry.[23,24] Where polysulfide shuttling in Li–S cells and the distribution of the polysulfide species within the cell has been investigated. In this work, *operando* electrochemical FLIM is demonstrated to spatially image the fluorescence lifetime of a graphite composite electrode within a Li-ion half-cell *vs.* lithium metal under potential control to spatially monitor changes in fluorescence lifetimes as function of potential.

FLIM was carried out on a Li|graphite half-cell within an *operando* spectroelectrochemical cell configuration, Fig. 1. The cell was composed of a free-standing graphite working electrode, glass fibre separator soaked with electrolyte, and a Li metal disk as the counter and reference electrode, Fig. S1. Two different electrolytes were selected for study: 1 M $Li[PF_6]$ in ethylene carbonate (EC): dimethyl carbonate (DMC) (1 : 1 v/v) and 1 M $Li[ClO_4]$ in EC: DMC (1 : 1 v/v). $Li[ClO_4]$ containing electrolytes tend to not have any significant background emission when

[a] *Stephenson Institute for Renewable Energy, Department of Chemistry, University of Liverpool, Liverpool, L69 7ZD, UK. E-mail: hardwick@liverpool.ac.uk*
[b] *Research Complex at Harwell, Rutherford Appleton Laboratory, Central Laser Facility, Harwell Science and Innovation Campus, Oxfordshire, OX11 0QX, UK*
[c] *The Faraday Institution, Quad One, Harwell Science and Innovation Campus, Didcot OX11 0RA, UK*

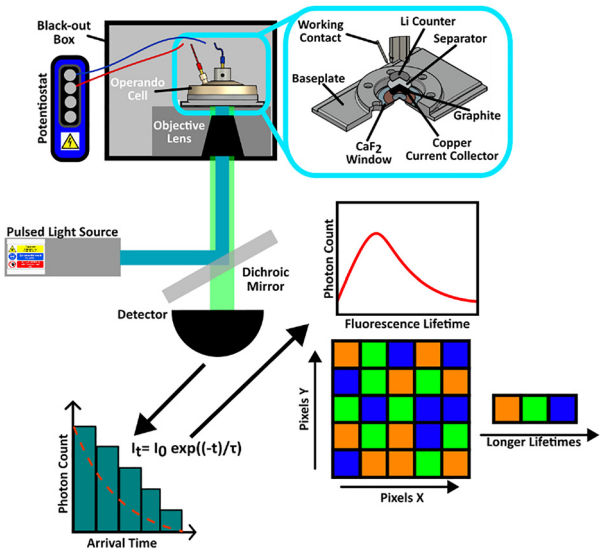

Fig. 1 Experimental setup. FLIM measurements are taken while simultaneously cycling the cell. The detector measures the decay in the intensity which is then converted to a population histogram and 2D colour map.

probed *via* Raman spectroscopy and have been used as model electrolytes.[9,10] Conversely, a Li[PF_6] containing electrolyte is selected due to the previously described, well-documented Raman baseline increases as well as being a standard salt in commercial Li-ion cells.[11] As the Li[ClO_4] containing electrolyte is not expected to generate fluorescing species, it is used as a control for comparison to Li[PF_6] during the FLIM measurements.

During *operando* FLIM measurements, the electrode was initially discharged from an open circuit potential (OCP) of 2.9 V *vs.* Li^+/Li at 0.2C to 5 mV *vs.* Li^+/Li, with a potential hold at 5 mV until the current had decayed to half the set C-rate (1C = 372 mAh g^{-1}, based on the theoretical capacity of graphite to form LiC_6), followed by a charge step to 1.5 V *vs.* Li^+/Li at 0.2C, Fig. S2. FLIM measurements were performed simultaneously by taking an image every 5 minutes, with an exposure time of 1 minute. Measurements and imaging were acquired using an inverted Nikon Ti–E microscope attached to a Nikon EC2 scanning unit. Microscopy images and FLIM measurements were acquired with a 10× (numerical aperture (NA) 0.3) or 100× (NA 0.9) air objectives providing spatial resolutions of 800 and 300 nm^2, respectively. Samples were illuminated with a diode pulsed laser, 40 ps, 405 nm wavelength operating at 80 MHz (BDS-SM, Becker and Hickl GmbH). A 450 nm long pass edge filter (Thorlabs) was used to eliminate the laser line. The scanning system, laser, and detector (PMC150) were linked *via* a single photon counting module (SPC150, Becker and Hickl GmbH) with a pixel dwell of 5 μs. Average fluorescence lifetimes were extracted using SPCImage software (version 9.0.73.0), Fig. S3, and a Python script was written to extract the photon count, Fig. S4.

Initially, a cell that deployed Li[ClO_4] as the electrolyte salt was monitored during cycling using the FLIM instrument. At OCP (*ca.* 2.9 V *vs.* Li^+/Li), the electrode exhibited low fluorescence with a photon count of 48 000 counts, Fig. S5, and the observed fluorescence had a short average lifetime of 350 ps, Fig. 2a. After cycling had been completed, Fig. 2b, no significant change in the lifetime distribution was observed and no new areas of the image displayed further fluorescence. Comparing the histograms of the population of decay lifetimes from before and after cycling, Fig. 2c, the general shape and size of the histogram was maintained. *Operando* FLIM measurements were collected whilst the potential was varied under galvanostatic control on the graphitic electrode. The average excited state

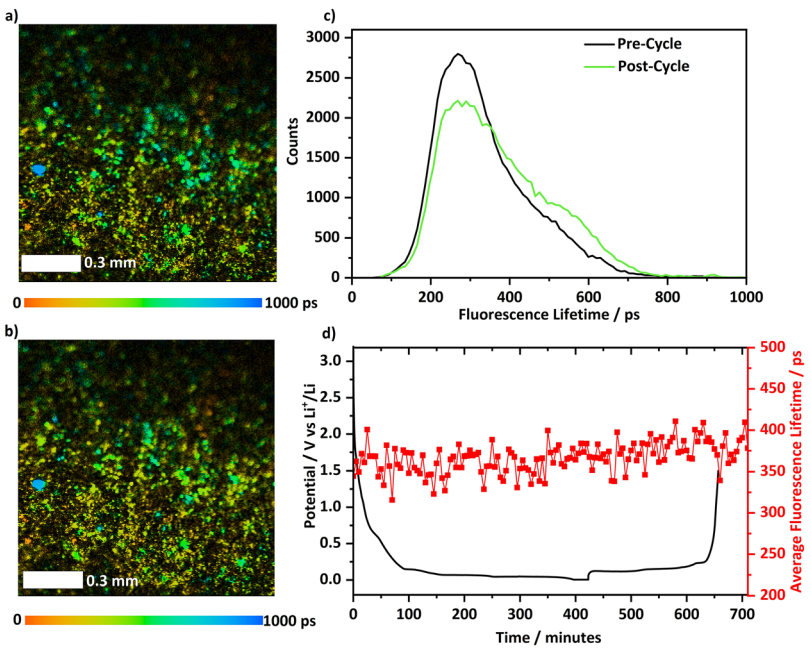

Fig. 2 FLIM analysis of the cell using a 1 M Li[ClO_4] EC/DMC (1 : 1 v/v) electrolyte. FLIM images of the surface of the electrode (a) before and (b) after cycling. (c) Histogram of the population of fluorescence lifetimes and (d) the change in the average lifetime of a function of electrochemical cycling.

lifetime of each measurement can be tracked as the electrode is cycled and is displayed in Fig. 2d with the voltage profile for lithium intercalation and extraction. Throughout cycling, the average lifetime fluctuates between a minimum of 310 ps and a maximum of 410 ps with no discernible pattern emerging during cycling. This shows, during cycling, species that affect fluorescence lifetime are not being created or consumed. At the end of cycling, the average lifetime remains stable (330–400 ps) during prolonged relaxation of the cell, Fig. S6. A change in photon count was recorded during cycling, Fig. S5. These are not significant enough (maximum variation of 500 counts) to indicate any change in the concentration of fluorescing species.

For the electrolyte containing Li[PF_6] as the salt, the initial FLIM measurement showed a decay histogram that was similar in shape to the initial FLIM measurement with the Li[ClO_4] as the electrolyte salt, Fig. S7. Note, whilst the Li[ClO_4] FLIM measurement was performed at a tenth of the magnification, the photon counts of both experiments are similar, Fig. S5.

Images of FLIM measurements before cycling and after cycling, Fig. 3a and b, show significant changes for the Li[PF_6]-based electrolyte. Fluorescence lifetimes become longer combining with the appearance of new areas becoming fluorescent, which indicates changes in species present on the electrode. The lifetime histogram collected post cycle, Fig. 3c, shows the species present have tended towards longer lifetime and with a greater range of lifetimes, indicating multiple species are present at the surface of the electrode, consistent with research showing that that SEI formation produces an inhomogeneous layer.[21]

Tracking the average lifetime of the fluorescent species as the cell was cycled, Fig. 3d, there is an initial systematic rise in the average lifetimes from 200 to 350 ps, which coincides with the potential relating to electrolyte solvent reduction as part of the SEI formation (from below 2 V down to 0.8 V *vs.* Li^+/Li). After the initial increase, the lifetime of species stabilises around 350 ps until the delithiation of graphite begins.

After this, the measured lifetime once again increases and rises to 450 ps. At the stage 2/stage 1 boundary (*ca.* 450 minutes) to the end of charge (*i.e.*, fully delithiated) the fluorescence lifetime fluctuated between 350–500 ps. The fluctuations indicate a dynamic process occurs during charge with species being both created and consumed that concurs with previous observations.[25] This can be further observed in Fig. S8, where individual fluorescence lifetime distributions presented as a function of the depth of lithiation show a greater change during the lithiation step between the two cells. Following a discharge–charge cycle, the cell was left to relax at OCP, Fig. S4, during which the lifetime decreases from 500 ps to between 400–425 ps and remains in this range. Additionally, the photon count, Fig. S6, remains relatively stable throughout cycling which was also observed with Li[ClO_4]-based electrolytes.

Importantly, changing the fitting model for the Li[PF_6] system, by adjusting the instrument response function, Fig. S9, reproduces the general pattern of the result – with a shift in the actual lifetime to longer lifetime by *ca.* 300 ps – lending confidence to the result.

The change in fluorescence lifetime of the cell deploying Li[PF_6] supports previous observations through Raman spectroscopy that Li[PF_6] reaction products generated during electrochemical cycling fluoresce.[11,15,26] The outcomes from this initial FLIM investigation highlights how future studies could be designed to observe correlation between fluorescence lifetimes and cell performance, and if fluorescence lifetime could be an indicator of the state of health of

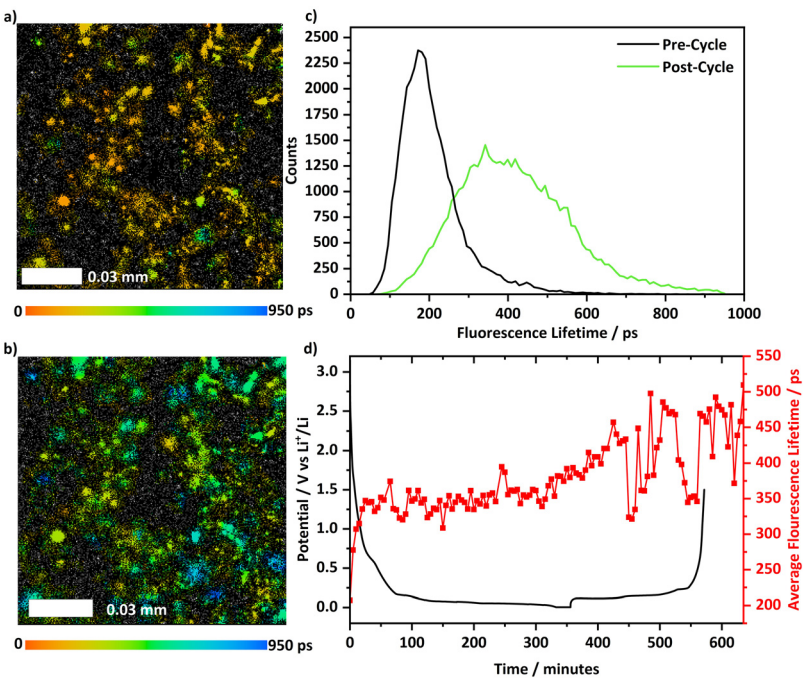

Fig. 3 FLIM analysis of the cell using a 1 M Li[PF_6] EC/DMC (1 : 1 v/v) electrolyte. FLIM images of the surface of the electrode (a) before and (b) after cycling. (c) Histogram of the population of fluorescence lifetimes and (d) the change in the average lifetime of species as a function of electrochemical cycling.

a Li-ion cell. The methodology provides an opportunity to resolve a key question on whether these side reaction products observed through fluorescence changes are detrimental to Li-ion cell performance, or just an inconvenience for monitoring cell chemistry *via* Raman microscopy.

While FLIM can show changes are occurring at the region around the porous electrode, identification of species is not possible using FLIM alone. However, the combination of this methodology with a fluorescence suppression methodology, for example a combined Kerr-gated or time gated Raman spectroscopy-FLIM technique may be able to elucidate the chemical nature in the future. FLIM could also be used to study SEI evolution due to lithium plating or elevated cell temperature.

Operando FLIM has been shown to be an effective method for monitoring the evolution of fluorescence lifetimes at the graphite/electrolyte interface during early electrochemical cycling. By combining FLIM with electrochemical cycling for *operando* study of the battery electrode surface, changes in the fluorescence lifetime of species and the generation of new long lifetime species were observed and correlated to electrochemical processes including SEI formation and evolution. Additional work will be required to understand how fluorescence lifetimes vary over successive cycles to relate to cell/electrode health and within a greater variety of electrolytes. At this current time, identification of species is not possible and will form the bulk of future studies combining with other techniques, such as Kerr-gated Raman. However, these current findings demonstrate the suitability of FLIM for *operando* studies of electrochemical systems and creates a further avenue to determine the role these low concentration fluorescing species have on a variety of battery chemistries and electrolytes.

MJQ: formal analysis, investigation, methodology, writing original draft manuscript, review and editing, and visualisation. TS: investigation, review and editing of manuscript. ARN: investigation, supervision, methodology, writing manuscript, review, and editing, and visualisation. OJB: methodology, SWB: methodology, review and editing. LJH: conceptualisation, investigation, funding acquisition, project administration, supervision, writing manuscript, review and editing.

LJH acknowledges financial support from the Faraday Institution CATMAT (FIRG016) and Degradation (FIRG024) projects and STFC for access to the FLIM within the OCTOPUS facility.

Conflicts of interest

The Authors declare that there were no conflicts of interest.

Data availability

The data supporting this article have been included as part of the supplementary information (SI). Supplementary information is available. See DOI: **https://doi.org/10.1039/d5cc04045k**.

References

1 B. Heid, P. Hertzke, P. Schaufuss, M. Wilthaner, J. Augustin, F. Kley, D. Schmid, L. Torscht, P. Pluijm, M. Stuchtey, C. Klein, T. Vahle, S. Buttkereit, A. Plieninger, M. Dirksmeier, M. Stanislaus, J. Eckart, E. Kemene, A. Zaragoza and A. Swierkowska, WEF A Vision for a Sustainable Battery Value Chain in 2030 Report, 2019.
2 Y. Gu, E.-M. You, J.-D. Lin, J.-H. Wang, S.-H. Luo, R.-Y. Zhou, C.-J. Zhang, J.-L. Yao, H.-Y. Li, G. Li, W.-W. Wang, Y. Qiao, J.-W. Yan, D.-Y. Wu, G.-K. Liu, L. Zhang, J.-F. Li, R. Xu, Z.-Q. Tian, Y. Cui and B.-W. Mao, *Nat. Commun.*, 2023, **14**, 3536.
3 T. M. M. Heenan, I. Mombrini, A. Llewellyn, S. Checchia, C. Tan, M. J. Johnson, A. Jnawali, G. Garbarino, R. Jervis, D. J. L. Brett, M. Di Michiel and P. R. Shearing, *Nature*, 2023, **617**, 507–512.
4 X. Liu, L. Yin, D. Ren, L. Wang, Y. Ren, W. Xu, S. Lapidus, H. Wang, X. He, Z. Chen, G.-L. Xu, M. Ouyang and K. Amine, *Nat. Commun.*, 2021, **12**, 4235.
5 A. R. Neale, D. C. Milan, F. Braga, I. V. Sazanovich and L. J. Hardwick, *ACS Energy Lett.*, 2022, **7**, 2611–2618.
6 R. Baddour-Hadjean and J.-P. Pereira-Ramos, *Chem. Rev.*, 2010, **110**, 1278–1319.
7 P. Novák, D. Goers, L. Hardwick, M. Holzapfel, W. Scheifele, J. Ufheil and A. Würsig, *J. Power Sources*, 2005, **146**, 15–20.
8 L. J. Hardwick, M. Hahn, P. Ruch, M. Holzapfel, W. Scheifele, H. Buqa, F. Krumeich, P. Novák and R. Kötz, *Electrochim. Acta*, 2006, **52**, 675–680.
9 J.-C. Panitz, F. Joho and P. Novák, *Appl. Spectrosc.*, 1999, **53**, 1188–1199.
10 C. Sole, N. E. Drewett and L. J. Hardwick, *Faraday Discuss.*, 2014, **172**, 223–237.
11 A. R. Neale, I. V. Sazanovich and L. J. Hardwick, *Curr. Opin. Electrochem.*, 2024, **45**, 101480.
12 Y. Domi, T. Doi, H. Nakagawa, T. Yamanaka, T. Abe and Z. Ogumi, *J. Electrochem. Soc.*, 2016, **163**, A2435.
13 Y. Ha, B. J. Tremolet De Villers, Z. Li, Y. Xu, P. Stradins, A. Zakutayev, A. Burrell and S.-D. Han, *J. Phys. Chem. Lett.*, 2020, **11**, 286–291.
14 R. Kostecki, L. Norin, X. Song and F. McLarnon, *J. Electrochem. Soc.*, 2004, **151**, A522–A526.
15 L. Cabo-Fernandez, A. R. Neale, F. Braga, I. V. Sazanovich, R. Kostecki and L. J. Hardwick, *Phys. Chem. Chem. Phys.*, 2019, **21**, 23833–23842.
16 A. Jarry, S. Gottis, Y.-S. Yu, J. Roque-Rosell, C. Kim, J. Cabana, J. Kerr and R. Kostecki, *J. Am. Chem. Soc.*, 2015, **137**, 3533–3539.
17 K. Suhling, L. M. Hirvonen, J. A. Levitt, P.-H. Chung, C. Tregidgo, A. Le Marois, D. A. Rusakov, K. Zheng, S. Ameer-Beg, S. Poland, S. Coelho, R. Henderson and N. Krstajic, *Biomed. Photonics*, 2015, **27**, 3–40.
18 J. M. Paredes, M. D. Giron, M. J. Ruedas-Rama, A. Orte, L. Crovetto, E. M. Talavera, R. Salto and J. M. Alvarez-Pez, *J. Phys. Chem. B*, 2013, **117**, 8143–8149.
19 H. Wallrabe and A. Periasamy, *Curr. Opin. Biotechnol*, 2005, **16**, 19–27.
20 S. W. Botchway, A. W. Parker, R. H. Bisby and A. G. Crisostomo, *Microsc. Res. Tech.*, 2008, **71**, 267–273.
21 S. J. An, J. Li, C. Daniel, D. Mohanty, S. Nagpure and D. L. Wood, *Carbon*, 2016, **105**, 52–76.
22 P. Verma, P. Maire and P. Novák, *Electrochim. Acta*, 2010, **55**, 6332–6341.
23 K. Coke, M. J. Johnson, J. B. Robinson, A. J. E. Rettie, T. S. Miller and P. R. Shearing, *ACS Appl. Mater. Interfaces*, 2024, **16**, 20329–20340.
24 N. A. Padilla, M. T. Rea, M. Foy, S. P. Upadhyay, K. A. Desrochers, T. Derus, K. A. Knapper, N. H. Hunter, S. Wood, D. A. Hinton, A. C. Cavell, A. G. Masias and R. H. Goldsmith, *ACS Sens.*, 2017, **2**, 903–908.
25 Y. Li, W. Chen, T. Lei, H. Xie, A. Hu, F. Wang, J. Huang, X. Wang, Y. Hu, C. Yang and J. Xiong, *Energy Storage Mater.*, 2023, **59**, 102765.
26 D. Martín-Yerga, D. C. Milan, X. Xu, J. Fernández-Vidal, L. Whalley, A. J. Cowan, L. J. Hardwick and P. R. Unwin, *Angew. Chem., Int. Ed.*, 2022, **61**, e202207184.